Analyst

RSC Publishing

PAPER

View Article Online
View Journal | View Issue

Cite this: *Analyst*, 2013, **138**, 1067

Conjugated self-doped polyaniline–DNA hybrid as trigger for highly sensitive reagentless and electrochemical self-signal amplifying DNA hybridization sensing

Yuwei Hu, Tao Yang,* Qianhe Li, Qian Guan and Kui Jiao*

In very recent years, polyaniline or its derivatives have been adopted to efficiently immobilize probe DNA *via* π–π interaction between conjugated interface and DNA bases. In this work, self-doped polyaniline (SPAN)–DNA hybrid was adopted as the platform to construct a DNA biosensor with label-free, reagentless and electrochemical self-signal amplifying features. This was achieved by the π–π interaction between conjugated SPAN and DNA bases, also the intrinsic differences between single-stranded DNA (ssDNA) and double-stranded DNA (dsDNA). The tightly cross-linked hybrid was tethered to Au electrode, which had been anchored by *p*-aminothiophenol (PATP) self-assembled monolayer (SAM) previously, based on the phosphoramidate bond between PATP and ssDNA. SPAN in the recognition surface exhibited well-defined redox signals under neutral conditions. Due to the intrinsic property differences between ssDNA and dsDNA, such as rigidity, π-stacked bases, charge distribution and long-range electron transfer, SPAN–DNA underwent a major conformational change after hybridization. The redox behaviors of SPAN were modulated by DNA, which served as signals to monitor hybridization. As an example, the gene fragment related to one of the screening genes for the genetically modified plants, cauliflower mosaic virus 35S gene was satisfactorily detected with this strategy. Under optimal conditions, the dynamic range for the DNA assay was from 1.0×10^{-14} mol L^{-1} to 1.0×10^{-8} mol L^{-1} with the detection limit of 2.3×10^{-15} mol L^{-1}. This work presents the construction of a recognition surface for the highly-sensitive electrochemical DNA hybridization detection *via* the self-signal amplifying procedure of conjugated SPAN–DNA hybrid. Unlike most signal amplifying processes using outer indicators, complex labels or other reagents, this procedure possesses simplicity and convenience.

Received 6th November 2012
Accepted 11th December 2012

DOI: 10.1039/c2an36620g

www.rsc.org/analyst

Introduction

DNA analysis plays an ever-increasing role in a number of areas related to human health such as diagnosis of infectious diseases, genetic mutations, clinical disease diagnostics and treatment. In this regard, nucleic acid assay technologies, which rely on the anchoring of multiple specific probe DNA fragments or oligonucleotides (ODNs) onto solid surfaces and detection of fluorescent or radioactively labeled analyte ODNs, appear as promising tools for the simultaneous analysis of multiple DNA sequences.[1] Although these technologies have the advantage of increased sensitivity to DNA detection, they need the incorporation of a labeling step into a nucleic acid assay, which has shortcomings of limited labeling efficiency, complex multi-step analysis and contamination to samples.[1,2] Since the procedures involved in label technologies prolong assay time and increase assay cost, many researches have been developing label-free technologies.[3,4] These methods, which detect the hybridization event through changes in the physical and chemical properties of the recognition layer, depend on changes of the optical[5,6] or electrochemical[7–9] signals.

At the same time, following the signal-amplifying principle, several other strategies have been successfully utilized for sensitive DNA hybridization assay, such as polymerase chain reaction,[10] nanoparticles,[11] enzymes,[12] and conjugated polymers (CPs).[13] The CPs-assisted signal-amplifying process is particularly effective, introducing multiple redox species per bind event and increasing the loading of capture probes.[14]

CPs own notable electrochemical and optical properties have been successfully employed in biosensing applications. The DNA detection based on CPs is very versatile and shows great promise of simplicity and high-sensitivity.[1] The conductive polymers, such as polypyrrole (PPy),[15–19] polymers of quinone

State Key Laboratory Base of Eco-chemical Engineering, College of Chemistry and Molecular Engineering, Qingdao University of Science and Technology, Qingdao 266042, China. E-mail: taoyang@qust.edu.cn; kjiao@qust.edu.cn; Fax: +86 532-84023927; Tel: +86 532-84022665

derivatives,[8,9,20–22] and polyaniline (PANI),[23–30] have been adopted to immobilize DNA probes *via* electrostatic adsorption, covalent bonding, or π–π interactions. Kim and coworkers[31] reported that CPs based biosensors were attractive approaches to improve the detection limit because an environmental change at a single site could affect the properties of the collective system, which produce large signal amplification. They had devised a signal-amplifying DNA microarray which combines the signal-amplifying scheme of conjugated polymers and efficient on-chip DNA synthesis. Based on different electrostatic interactions and conformational structures between the CPs, and single-stranded DNA (ssDNA) or hybridized double-stranded DNA (dsDNA), Leclerc and coworkers detected and distinguished a specific sequence of oligonucleotides at very low concentrations.[32] Polymers bound to dsDNA underwent a major conformational change in comparison to when they bound to ssDNA. He and Zheng reported the use of a polythiophene derivative in conjunction with metallic striped nanorods for multiplexed DNA detection that enables simultaneous monitoring of multiple biological recognition events in a label-free fashion.[33] In very recent years, it should be noted that, polyaniline or its derivatives, owning rich-conjugated structures, functional groups, and excellent electrochemical activity, have efficiently immobilized the probe DNA through π–π interactions between conjugated interface and DNA bases. After hybridization, the resulting dsDNA will release from conjugated interface, inducing signal changes (signal-on or signal-off). The signal changes could serve as a powerful tool for sensitive detection of the gene sequences.[34,35]

As one of the derivatives of polyaniline (PANI), self-doped polyaniline (SPAN) contains conjugated π–π structure and overcomes the major drawbacks of traditional PANI, such as its poor solubility in aqueous solution and the loss of electrochemical activity in solutions of pH greater than 4.[36] Therefore, it could be adopted to detect bio-analytes at physiological pH. SPAN has acted as a supporting platform for the impedance sensing of DNA hybridization by our group.[37–39]

In the present work, SPAN was adopted as the platform to conduct a label-free, electrochemical self-signal amplifying DNA hybridization assay. The negatively charged SPAN was mixed with Al(III) at a certain volume ratio to form a SPAN–Al(III) mixture. Based on the π–π interactions, electrostatic force and adsorption effect, ssDNA could form a hybrid with the SPAN–Al(III) mixture, denoted as SPAN–ssDNA. In the hybrid formation process, Al(III) served as a bridging medium[40] (Scheme 1). Then, the recognition surface capable of detecting specific sequences of DNA was achieved by tethering the SPAN–ssDNA hybrid to Au electrode *via* an anchoring self-assembled monolayer (SAM) of *p*-aminothiophenol (PATP) through the phosphoramidate bond between 5′-phosphate group of DNA sequence and $-NH_2$ of PATP. SPAN in the hybrid exhibited a well-defined redox signal in neutral solution (Scheme 1, blue curve (i)). After the recognition surface hybridized with complementary DNA sequence, an amplified self-signal of SPAN (Scheme 1, red curve (ii)) was observed corresponding to the formation of SPAN–dsDNA hybrid. SPAN bound to dsDNA underwent major interfacial and electrochemical property changes. These intrinsic changes transformed DNA hybridization events into detectable electrochemical signals, which could be easily monitored by electrochemical technologies. For investigating the viability of this approach, the gene fragment related to cauliflower mosaic virus 35S gene (CaMV35S), one of the promoters in the genetically modified plants, was detected.

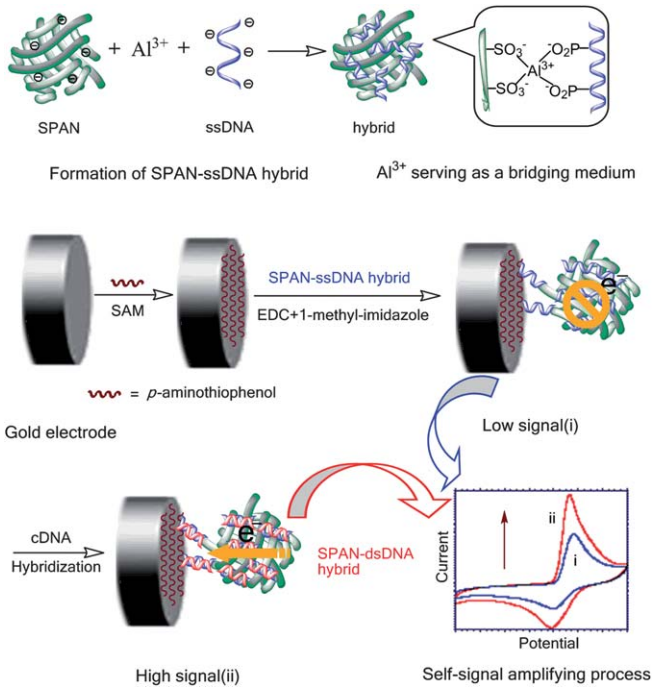

Scheme 1 Schematic representation of the construction of conjugated SPAN–DNA hybrid and the electrochemical self-signal amplifying DNA hybridization detection.

Materials and methods

Apparatus and chemicals

All electrochemical experiments were conducted in a conventional three-electrode cell at room temperature using a CHI 660B electrochemical workstation (Shanghai CH Instrument Company, China). A Pt wire and a saturated calomel electrode (SCE) were used as counter electrode and reference electrode, respectively. Au electrode (2 mm diameter) and the modified Au electrodes were used as the working electrode. Scanning electron microscopy (SEM) was carried out using a JSM-5900 machine (JEOL, Tokyo, Japan).

SPAN (copolymer of aniline and *m*-aminobenzenesulfonic acid) nanofibres were prepared according to ref. 41. PATP (purity >97%) and 1-(3-dimethylaminopropyl)-3-ethylcarbodiimide hydrochloride (EDC) were purchased from Sigma-Aldrich (USA). Piranha solution (v/v 3 : 1 concentrated H_2SO_4/30% H_2O_2). The other usual reagents were purchased from the Shanghai Chemical Reagent Co. (Shanghai, China) and were all of analytical reagent grade. Solutions were all prepared with Aquapro ultrapure water (Aquaplus AWL-1002-P, Ever Young Enterprises Development Co. Ltd, Chongqing, China).

The 18-base synthetic oligonucleotides probe, its complementary sequence DNA (cDNA, target DNA, namely an 18-base fragment of CaMV35S gene sequence), double-base mismatched DNA and non-complementary (ncDNA) were synthesized by Beijing SBS Gene Technology Co. Ltd (Beijing, China). Their base sequences were as follows:

probe DNA (ssDNA): 5′-TCT TTG GGA CCA CTG TCG-3′

target DNA (cDNA): 5′-CGA CAG TGG TCC CAA AGA-3′

double-base mismatched DNA: 5′-CGA ***A***AG TGG TCC ***G***AA AGA-3′

ncDNA: 5′-GCA TCG AGC GAG CAC GTA-3′.

All oligonucleotides stock solutions of 18-base oligomers (1.0×10^{-6} mol L^{-1}) were prepared using Tris–HCl solution (5.0 mmol L^{-1} Tris–HCl, 50.0 mmol L^{-1} NaCl, pH 7.0), which were stored at 4 °C. More diluted solutions were obtained *via* diluting aliquot of the stock solution with ultrapure water prior to use. The hybridization solution was diluted with 2× SSC (pH 7.0), which consisted of 0.30 mol L^{-1} NaCl and 0.030 mol L^{-1} sodium citrate tribasic dihydrate ($C_6H_5Na_3O_7 \cdot 2H_2O$).

Preparation of SAM modified Au electrode

SAM modified Au electrode was fabricated according to the method of Ma.[42] In brief, the Au electrode was polished with a piece of emery paper, followed with 1.0, 0.3, and 0.05 μm α-Al_2O_3 paste, respectively. After being cleaned ultrasonically in 95% ethanol and acetone for 3 min, respectively, the electrode was chemically etched by being dipped in a piranha solution for 10 min to oxidize impurities, and then rinsed with ultrapure water. SAM was formed by immersing the pretreated bare Au electrode in 5 mmol L^{-1} PATP solution at 4 °C for 9 h. The PATP/Au electrode was then rinsed with ultrapure water, and dried under nitrogen gas.

Formation of the recognition surface

The formation of recognition surface was carried out with the following procedure: 400 μL 8 g L^{-1} SPAN nanofibres were mixed with 100 μL 5 mmol L^{-1} $Al(NO_3)_3$ solution (v/v 4 : 1) and then the mixture was sonicated for 30 min at ambient temperature. 100 μL 2×10^{-8} mol L^{-1} ssDNA solution was blended with the mixture (v/v 1 : 1) to form a hybrid, denoted as SPAN–ssDNA. The anchoring of SPAN–ssDNA on PATP/Au electrode was based on the phosphoramidate bond between 5′-phosphate group of DNA sequence and $-NH_2$ of PATP according to ref. 43. Then the recognition layer was washed with 0.2% sodium dodecyl sulfate (SDS) solution and ultrapure water. The electrode was denoted as SPAN–ssDNA/PATP/Au.

DNA hybridization reaction

DNA hybridization reaction was conducted by dropping 5 μL of appropriate concentration of target DNA solution onto the recognition surface and allowed reaction for 30 min. Then the electrode was washed with 0.2% SDS solution to remove the unhybridized DNA and this hybridized electrode was denoted as SPAN–dsDNA/PATP/Au. The same procedure as mentioned above was applied to the probe-modified electrode for hybridization with double-base mismatched and ncDNA sequences.

Electrochemical measurements

The following parameters were employed for cyclic voltammetry (CV): scan rate 100 mV s^{-1} (unless otherwise indicated), potential scanning range +0.8 to −0.6 V. Supporting electrolyte was 0.30 mol L^{-1} phosphate buffer solution (PBS pH 7.0).

The electrochemical impedance spectroscopy (EIS) experimental parameters: the AC voltage amplitude was 5 mV and the voltage frequencies ranged from 0.05 Hz to 10^4 Hz. The applied potential was selected as 0.172 V (*vs.* SCE) corresponding to ferrocyanide/ferricyanide half-wave potential. The supporting electrolyte was 1.0 mmol L^{-1} $K_3[Fe(CN)_6]$ and 1.0 mmol L^{-1} $K_4[Fe(CN)_6]$ (1 : 1) solution containing 0.1 mol L^{-1} KCl.

Results and discussion

Morphology characterization of the hybrid

The morphology of chemically synthesized SPAN is shown in Fig. 1A. Coarse, cross-linked nanofibres with average diameter of 100 nm were observed. This morphology possessed large surface area which was beneficial to bind bioanalytes and facilitate electron transfer. After the formation of hybrid with ssDNA, more nanofibres twisted together and the surface of nanofibres became obviously smooth (Fig. 1B), which indicates the interaction between SPAN and ssDNA. When the SPAN nanofibres were mixed with Al(III), the electrical property of SPAN might be changed, which was propitious to the formation of hybrid with negatively charged ssDNA. Besides, due to the unique conjugated π-bond of SPAN and the exposed aromatic nucleotide bases of ssDNA, the π–π interactions[34] happened and associated ssDNA with SPAN. These interactions resulted in the SPAN–ssDNA hybrid through adsorbing ssDNA on the surface of SPAN. To further confirm these interactions, the concentration of SPAN was changed to 200 g L^{-1} keeping other conditions unaltered. The morphology of these nanofibres is shown in Fig. 1C. Although the nanofibres' surface was smoother than that in Fig. 1A (without the formation of hybrid

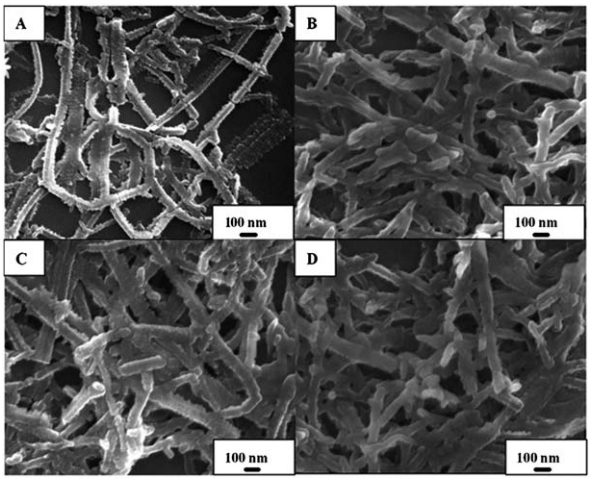

Fig. 1 SEM images of SPAN nanofibres (A), SPAN–ssDNA hybrid with different concentrations of SPAN: 8 g L^{-1} (B), 200 g L^{-1} (C) and SPAN–dsDNA hybrid with 8 g L^{-1} SPAN (D).

with ssDNA), it was not as smooth as that in Fig. 1B. Due to the high concentration of SPAN, comparatively less ssDNA might bind to the polymer matrix, which results in the less smooth surface. The morphology of SPAN–dsDNA hybrid is shown in Fig. 1D. No obvious change of the morphology could be observed compared to that of SPAN–ssDNA hybrid.

CV based characterization of recognition surfaces

The effect of ssDNA within the recognition surface on the electrochemical behaviors of SPAN was investigated and is presented in Fig. 2 and Table 1. Fig. 2 shows the CVs of SAM modified Au electrode (curve a), SPAN nanofibres modified bare Au electrode (curve b), SPAN modified SAM Au electrode (curve c) and SPAN–ssDNA hybrid covalently immobilized on SAM Au electrode (curve d) in 0.3 mol L^{-1} PBS (pH 7.0). No redox peaks were observed at PATP/Au, which elucidated that no redox reaction occurred at the electrode surface. A couple of well-defined peaks according to the redox process of azo group in SPAN[44] were observed in the potential range of −0.2 to 0 V (curves b, c and d). The formal potential of the redox SPAN in the SPAN–ssDNA hybrid ($E^{\circ\prime}$ of −0.079 V *vs.* SCE, Table 1), evaluated from the mean of the oxidation and reduction peak potentials, was sufficiently negative to avoid damaging the ssDNA sequences through oxidation of guanine and adenine bases.[45] The 0.029 V decrease of $E^{\circ\prime}$ of the redox SPAN in the presence of ssDNA indicated an interaction existed between the ssDNA and the redox SPAN.[46] An increase in the separation of anodic and cathodic peak potentials (ΔE_p) from 0.143 V to 0.166 V at this scan rate indicates a decrease in the rate of the electron transfer for the SPAN–ssDNA hybrid (the ΔE_p of SPAN recorded at bare Au electrode is also listed in Table 1 for comparison). When scan rate ≤100 mV s^{-1}, SPAN redox peak currents were directly proportional to the scan rate, meaning an indication of a surface confined redox process.[47] According to the equation, $I_p = n^2F^2\Gamma Av/4RT$ and $Q_\Gamma = nFA\Gamma_{azo}$, where n is the number of electron transfer, F is Faraday's constant, and A is the electrode area, v is scan rate and other parameters have their usual meanings,[47] the electron transfer number and the azo group surface coverage (Γ_{azo}) for redox SPAN alone and SPAN–ssDNA hybrid were calculated and are listed in Table 1. The electron transfer number of redox SPAN recorded at bare Au was evaluated to be 1.93, which is closer to 2 than that of SPAN at PATP/Au and in the SPAN–ssDNA hybrid modified PATP/Au. This might be attributed to the presence of PATP and the flexible characteristics and negatively charged phosphate backbones of the ssDNA. After the formation of SPAN–ssDNA hybrid, ssDNA wrapped around SPAN, changed the interfacial properties and blocked the effective electron transfer along the SPAN chains pathways.

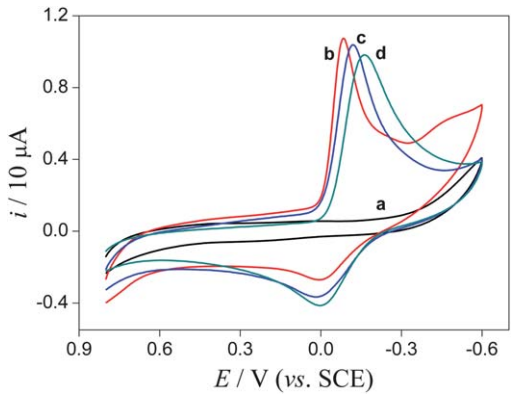

Fig. 2 CVs of PATP/Au (a), SPAN/Au (b), SPAN/PATP/Au (c), and SPAN–ssDNA/PATP/Au (d). Scan rate, 100 mV s^{-1}, supporting electrolyte, 0.3 mol L^{-1} PBS (pH 7.0).

The Γ_{azo} for the SPAN–ssDNA hybrid at SAM modified Au electrode was calculated as 3.17×10^{-9} mol cm^{-2}, which is higher than that of SPAN at bare Au and PATP/Au electrode, which is 2.63×10^{-9} mol cm^{-2} and 2.74×10^{-9} mol cm^{-2}, respectively (Table 1). Because no special interactions existed between SPAN and bare Au electrode, the SPAN nanofibres could hardly bind to the electrode surface, which results in the lower value of Γ_{azo}. It can be seen that the Γ_{azo} of SPAN at PATP/Au was a bit higher than that at bare Au. This might be ascribed to the ordered SAM increasing the immobilization amount of SPAN nanofibres, however, the effect was not obvious and effective. While for the SPAN–ssDNA hybrid, the interactions between the two species with Al(III) as the bridging medium could make SPAN nanofibres bind easily to the electrode surface. In this conformation, ssDNA might act as cross-linker and increase the steric density of SPAN nanofibres. Besides, the mercapto group of PATP molecules has an intensive interaction with the Au electrode, while the amino group cannot directly interact with Au electrode. Therefore, PATP molecule might be perpendicularly linked to the Au electrode surface and ordered, tightly packed SAM was formed. When the SPAN–ssDNA hybrid was immobilized on the SAM modified electrode, the good orientation of covalent binding and high steric density of SPAN increased the immobilized amount and stability of SPAN nanofibres, which is beneficial to detect bioanalytes.

EIS based characterization of recognition surfaces

In the electrochemical biosensing field, EIS is a valuable technique for characterizing surface modifications, such as the immobilization of polymers or biomolecules on the transducer,[48] and would be sensitive to the interfacial changes accompanying DNA hybridization. In order to obtain more information from EIS results, the recognition surface modified electrode was modeled using a Randles equivalent circuit (inset of Fig. 3). Where, R_s is the electrolyte solution resistance, R_{et} is the element of interfacial electron transfer resistance, and W is the Warburg impedance resulting from the diffusion of ions. A constant phase element (in parallel with W and R_{et}) acts as a non-ideal capacitor, which is commonly adopted to account for inhomogeneities on the electrode surface.[49] The semicircle diameter of the Nyquist diagram equals R_{et}. In this section, EIS was adopted to investigate the properties of recognition surfaces using $[Fe(CN)_6]^{3-/4-}$ as the traditional redox indicator. The Nyquist plots recorded at various modified electrodes are shown in Fig. 3. Curve a was the Nyquist diagram of $[Fe(CN)_6]^{3-/4-}$ at bare Au electrode. The high frequency section of the curve

Table 1 Electrochemical parameters for redox SPAN alone and SPAN–ssDNA hybrid recorded by CV in 0.3 mol L^{-1} PBS (pH 7.0)

Parameter	SPAN/Au	SPAN/PATP/Au	SPAN–ssDNA/PATP/Au
$E^{o\prime}$ (V)	−0.040	−0.050	−0.079
ΔE_p (V)	0.090	0.143	0.166
n	1.93	1.85	1.79
Γ_{azo} (mol cm^{-2})	2.63×10^{-9}	2.74×10^{-9}	3.17×10^{-9}

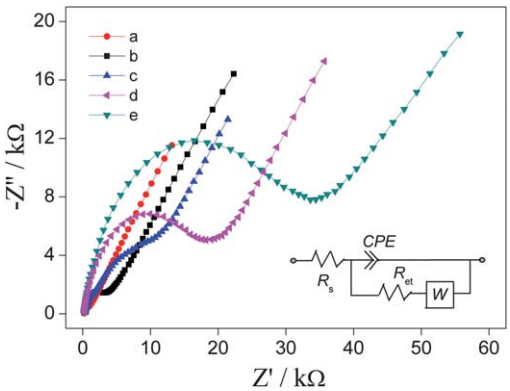

Fig. 3 Nyquist plots recorded at bare Au electrode (a), PATP/Au SAM electrode (b), SPAN modified SAM electrode (c), SPAN–ssDNA hybrid modified SAM electrode (d), and SPAN–dsDNA hybrid modified SAM electrode (e). Supporting electrolyte solution was 1.0 mmol L^{-1} $K_3[Fe(CN)_6]$ and 1.0 mmol L^{-1} $K_4[Fe(CN)_6]$ (1 : 1) solution containing 0.1 mol L^{-1} KCl. Inset: equivalent circuit used to model impedance data in the presence of redox couples.

shows an arc, the diameter of which displays the interfacial electron transfer resistance $R_{et} = 7.80 \times 10^2$ Ω. Curve b was the Nyquist diagram at the PATP/Au SAM electrode with its R_{et} value of 3.12×10^3 Ω. Compared with curve a, the R_{et} value of curve b increased markedly. These experimental results demonstrate that the SAM of PATP on Au surface could block the electron transfer of $[Fe(CN)_6]^{3-/4-}$. When SPAN nanofibres were immobilized on PATP/Au, the Nyquist diagram changed to curve c with the R_{et} value of 1.12×10^4 Ω, which was likely ascribed to the sulfonic group. After SPAN–ssDNA hybrid was covalently immobilized on PATP/Au SAM electrode, the Nyquist diagram of $[Fe(CN)_6]^{3-/4-}$ at this modified electrode is shown in curve d with the R_{et} value of 1.82×10^4 Ω. Compared with curve c, the R_{et} value of curve d further increased. This change of the Nyquist diagram during the modification process elucidated an increased amount of negative charges of the electrode surface, which was strong proof that the SPAN–ssDNA hybrid had been successfully immobilized on the electrode surface. The abundant electronegative phosphate backbones of DNA sequences prevented $[Fe(CN)_6]^{3-/4-}$ effectively from reaching the electrode surface for electron transfer during the process of redox reaction. After hybridization of the probe DNA with cDNA, the Nyquist diagram of $[Fe(CN)_6]^{3-/4-}$ is shown in curve e with the R_{et} value of 3.36×10^4 Ω. The increased value of R_{et}, compared with that of curve d, exhibited the more negative charges on the electrode surface, which elucidated the formation of SPAN–dsDNA hybrid.

Stability of recognition surface

Stability of the recognition surface is a key factor in transduction of the DNA hybridization event. The stability of the SPAN–ssDNA hybrid tethered to the PATP/Au electrode was evaluated and compared to that of the hybrid immobilized on bare Au electrode (Fig. 4).

After being dipped in 0.3 mol L^{-1} PBS (pH 7.0) for 1 h, the peak current, normalized to time zero,[46] of the SPAN–ssDNA hybrid tethered to the PATP/Au electrode decreased by 3%, which was significantly less than that for the hybrid adsorbed on bare Au electrode, at 10%. A similar trend was observed after 5 h, with the normalized currents of 92% and 69% for SPAN–ssDNA hybrid on PATP/Au and bare Au, respectively. After 10 h, the normalized currents decreased by 15% and 44% for the hybrid on PATP/Au and bare Au, respectively. It was worth noting that, with the prolonging of dipping time, peak current of SPAN–ssDNA hybrid tethered to PATP/Au electrode decreased softly while for that of the hybrid adsorbed on bare Au it decreased drastically. Due to the poor binding force of the hybrid on bare Au electrode, films might drop easily from the electrode surface. Based on the SAM, SPAN–ssDNA hybrid could be covalently tethered to the PATP/Au electrode surface *via* the phosphoramidate bond between PATP and ssDNA, which elucidated an excellent stability. However, the peak current still exhibited a downward trend over a 10 h period of being dipped in 0.3 mol L^{-1} PBS (pH 7.0). This might be ascribed to the high ionic strength in the PBS. Different kinds of ion, such as Na^+, K^+,

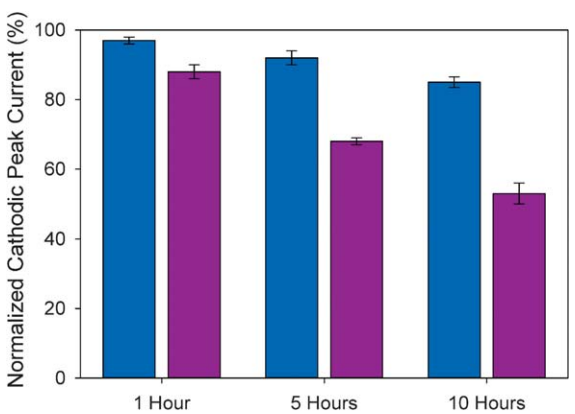

Fig. 4 Stability of peak current measurements from CVs of the SPAN–ssDNA hybrid tethered on PATP/Au (left, blue) and bare Au (right, brown) electrodes over a 10 h period of being dipped in 0.3 mol L^{-1} PBS (pH 7.0). Peak currents were recorded from CVs in the same solution at 100 mV s^{-1} and were normalized to their values at time zero.

Cl^-, HPO_4^{2-}, $H_2PO_4^-$, exhibited the competitive inhibition and attenuated the interactions between ssDNA and SPAN, which could result in SPAN leaving the recognition surface.

Optimization of assembly time and selection of volume ratio of Al(III) ion to SPAN

The assembly time, which might affect the formation and packing density[50] of the PATP SAM, was optimized in detail. The bare Au electrode was immersed in an ethanol solution of 5 mmol L^{-1} PATP at 4 °C for different times, followed by rinsing the electrode with ultrapure water and then drying it under nitrogen gas. The Nyquist diagram of $[Fe(CN)_6]^{3-/4-}$ at the SAM modified Au electrode was recorded. The difference of R_{et} (ΔR_{et}) between the bare Au electrode and the SAM modified Au electrode was calculated to evaluate the effect of self-assembled time. With the prolongation of assembly time, the value of ΔR_{et} increased accordingly. However, ΔR_{et} changed little after 9 h. Considering assembly effect and time-saving, 9 h was chosen as the self-assembled time.

It is well-known that the interaction between Al(III) and phosphate groups is very strong.[51] In this system, Al(III) ion acts as an important factor in the formation of SPAN–ssDNA hybrid. As the amount of Al(III) ion could affect the electrical property of SPAN and the binding force between SPAN–Al(III) and DNA sequences. Different volume ratios of Al(III) ion to SPAN in the mixture were investigated, such as 4 : 1, 2 : 1, 1 : 1, 1 : 2, 1 : 3, 1 : 4 and 1 : 5. After sonication of the mixture, ssDNA solution was blended with it (v/v 1 : 1). Then the SPAN–ssDNA hybrid was covalently immobilized on PATP/Au electrode and electrochemical behaviors were investigated by CV in PBS (pH 7.0). With the decrease of volume ratio of Al(III) ion to SPAN, the redox peak currents of SPAN increased accordingly. The maximum redox peak currents were observed at the ratio of 1 : 4 and then decreased with further decreasing the volume of Al(III). If the volume ratio of Al(III) ion to SPAN was too high, there would be extra Al(III) ions in the mixture. When ssDNA solution was blended with the mixture, extra Al(III) ions might bind to ssDNA. There may exist a competition between extra Al(III) ions and SPAN–Al(III) mixture to bind to ssDNA, which results in the formation of poor amounts of SPAN–ssDNA hybrid. This meant that less hybrid would be covalently immobilized on the electrode surface and hence induced the low peak currents. A balance would be achieved at the volume ratio of 1 : 4, where most Al(III) ion bound to SPAN and little Al(III) ion or SPAN existed alone. At this time, plenty of SPAN–ssDNA hybrids were formed and possessed good stability. However, if the volume ratio was lower than 1 : 4, extra SPAN would exist. Al(III) ion might be totally entrapped in these nanofibres, making it difficult for Al(III) ions to bind to ssDNA. Therefore, the SPAN–ssDNA hybrid would be inefficiently formed and the peak currents decreased. In our experiments, the volume ratio of Al(III) ion to SPAN was selected as 1 : 4.

Self-signal amplifying procedure for DNA hybridization

After hybridization of the DNA probe with cDNA, the CV curve of SPAN–dsDNA hybrid is shown in Fig. 5a. Compared with SPAN–ssDNA modified PATP/Au electrode (Fig. 2d), enhanced redox peak currents of SPAN–dsDNA hybrid were observed. It would be considered as significant signal for hybridization reactions. After the SPAN–ssDNA/PATP/Au hybridized with cDNA to form SPAN–dsDNA hybrid, the value of ΔE_p of SPAN was 0.136 V, which is less than that derived from the SPAN–ssDNA hybrid tethered electrode (0.166 V). These results could be strong proof that the hybridization event had successfully occurred.

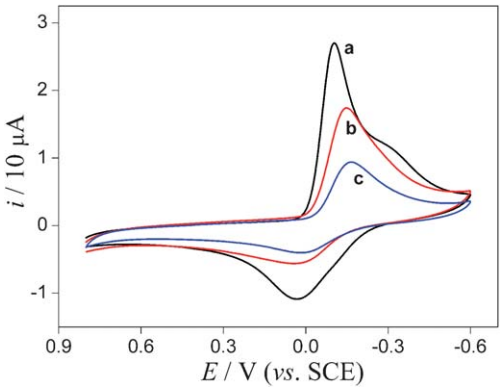

Fig. 5 CVs of the SPAN–ssDNA/PATP/Au hybridized with cDNA (a), the SPAN–ssDNA/PATP/Au hybridized with double-base mismatched DNA (b), the SPAN–ssDNA/PATP/Au hybridized with ncDNA (c) in 0.3 mol L^{-1} PBS (pH 7.0). Scan rate, 100 mV s^{-1}.

Two aspects should be considered to interpret the observed phenomena. When the hybridization event occurred, the base pair stacking between ssDNA and cDNA took place. A pathway for electron transfer along the double-helix structure was formed. It had been shown that the efficient long-range electron transfer occurred through the π-stacked bases of the double-helix structure over distances of up to 35 Å.[52] Due to the much higher rigidity of dsDNA compared to ssDNA, the electron transfer rate along the double-helix structure was faster than that along single-chain structures.[53] The other aspect could be interpreted as follows. According to the literature,[8] ssDNA behaves as a coil, has a high degree of freedom and is able to interact with molecules on the surface. Conversely, dsDNA is straight and rigid. The random and flexible ssDNA wraps around the SPAN nanofibres in the SPAN–ssDNA hybrid. These ssDNA random coils, which are bound to the SPAN nanofibres surface, were not beneficial to the electron transfer along the SPAN chains pathways and induced the low self-redox peak currents of SPAN. When the formation of hydrogen bonds between the bases of ssDNA and their complementary ones took place, the comparatively weaker π–π interactions between ssDNA and SPAN might be vanished. However, the hybridization reaction could not peel ssDNA off the SPAN nanofibres since the electrostatic forces still existed between the phosphate backbones and the sulfonic groups. The formed dsDNA could not bind to SPAN nanofibres as ssDNA did because of its straightness, rigidity and fully paired bases. Therefore, the restraint of electron transfer along SPAN chains pathways is interfered with because ssDNA was attenuated. The hybridization reaction created the double-helix structure and set the SPAN chains pathways partially free, both of which facilitated

the electron transfer and induced to the amplified self-redox signals of SPAN. Hence, the conformational, interfacial and electrochemical property changes from SPAN–ssDNA to SPAN–dsDNA hybrid transformed DNA hybridization into detectable electrochemical signals, which could be monitored by the label-free DNA biosensing assay. The result elucidated that a self-signal amplifying procedure for DNA hybridization detection could be achieved based on the SPAN–DNA hybrid.

The selectivity of the label-free, electrochemical self-signal amplifying DNA hybridization detection could be illustrated by using the SPAN–ssDNA hybrid tethered electrode to hybridize with different kinds of DNA sequences (including double-base mismatched and ncDNA sequences). The CVs were recorded and are shown in Fig. 5 (curve b and c). After hybridization with double-base mismatched sequences, the peak currents increased (curve b) compared with SPAN–ssDNA modified PATP/Au electrode (Fig. 2d). However, the increment of peak currents was much smaller than that obtained from the hybridization with cDNA (curve a). This might be ascribed to the fact that base mismatches essentially suppressed the long range electron transfer through a length of dsDNA.[54,55] When the SPAN–ssDNA hybrid tethered electrode was hybridized with ncDNA (curve c), the signal of CV varied little compared with that of curve d in Fig. 2, which meant no hybridization reaction occurred. These results suggest that the label-free, electrochemical self-signal amplifying DNA biosensing based on SPAN–DNA hybrid exhibits good selectivity.

Detection of sequence-specific CaMV35S gene fragment

The SPAN–ssDNA hybrid tethered SAM modified Au electrode was applied to detect the CaMV35S gene target sequence and the CVs were recorded after hybridization with different concentrations of the complementary target sequence (Fig. 6). The difference (namely Δi_{pc}) between the i_{pc} value of the probe-captured electrode and that after hybridization with cDNA was adopted as the measurement signal. The Δi_{pc} value was linear with the logarithm of the gene sequence concentrations (inset, Fig. 6). The dynamic determination range for the CaMV35S gene target sequence was from 1.0×10^{-14} mol L^{-1} to 1.0×10^{-8} mol L^{-1} with the regression equation: Δi_{pc} (10 μA) = 0.2713log C + 3.777, and the correlation coefficient: $\gamma = 0.9927$. The detection limit of this label-free DNA hybridization assay was 2.3×10^{-15} mol L^{-1} using 3σ (where σ was the relative standard deviation of 11 parallel measurements of the blank solution). Based on the SPAN–DNA hybrid self-signal amplifying strategy, the sensitivity for the CaMV35S gene sequence determination was greatly enhanced compared to previous work.[38,39]

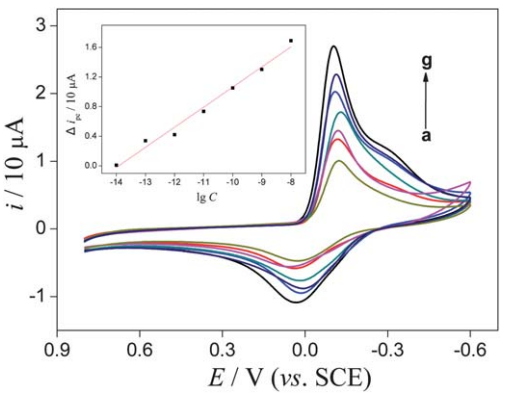

Fig. 6 CVs of the SPAN–ssDNA hybrid tethered PATP/Au electrode hybridized with its complementary CaMV35S gene sequences of 1.0×10^{-14} mol L^{-1} (a), 1.0×10^{-13} mol L^{-1} (b), 1.0×10^{-12} mol L^{-1} (c), 1.0×10^{-11} mol L^{-1} (d), 1.0×10^{-10} mol L^{-1} (e), 1.0×10^{-9} mol L^{-1} (f), 1.0×10^{-8} mol L^{-1} (g) recorded in 0.3 mol L^{-1} PBS (pH 7.0). Inset: the plot of Δi_{pc} *vs.* the logarithm of the gene sequence concentrations.

Regeneration of the recognition surface can be achieved by immersing the SPAN–dsDNA hybrid tethered PATP/Au electrode in 10 mmol L^{-1} NaOH (2 min),[48] followed by rinsing the electrode with ultrapure water. This treatment denatured the DNA double-helix. Repeat hybridization of this regenerated SPAN–ssDNA recognition surface with cDNA resulted in a CV signal magnitude >92% of the initial signal, which indicated that the SPAN–ssDNA hybrid was still tethered on the SAM modified Au electrode and could be used repetitively without much loss of its signal.

Reproducibility seems to be the key for the biosensing assay to practical applications. In our test, the reproducibility of this label-free, electrochemical self-signal amplifying DNA hybridization assay was examined by a parallel measurement method. Six parallel SPAN–ssDNA hybrid modified electrodes were performed and then hybridized, respectively, with 1.0×10^{-10} mol L^{-1} target DNA. CV determination for every electrode before and after DNA hybridization was recorded. A relative standard deviation of 2.41% for the Δi_{pc} value was obtained, which elucidates that the reproducibility of this DNA hybridization assay is good.

Conclusions

In this paper, the highly sensitive, label-free and electrochemical DNA hybridization assay was achieved by a novel and simple recognition surface, which consisted of SPAN nanofibres, Al(III) ion and ssDNA. With a SAM of PATP, the conjugated SPAN–ssDNA hybrid could be covalently tethered on the surface of Au electrode. After hybridization with cDNA, the SPAN–ssDNA changed to SPAN–dsDNA hybrid, which formed an effective electron transfer pathway. Based on the interfacial property differences of SPAN bound to ssDNA and dsDNA, owing to the rigidity, π-stacked bases, charge distribution and long-range electron transfer intrinsic differences between ssDNA and dsDNA, an amplified self-signal of SPAN was obtained after hybridization reaction. This could be easily detected by electrochemical techniques without any labeling steps. The CaMV35S gene target sequences were detected with this strategy with satisfactory results.

Acknowledgements

This work was supported by the National Natural Science Foundation of China (no. 21275084, 20975057, no. 20805025), Doctoral Foundation of the Ministry of Education of China (no.

20113719130001), Outstanding Adult-Young Scientific Research Encouraging Foundation of Shandong Province (no. BS2012CL013), and the Scientific and Technical Development Project of Qingdao (no. 12-1-4-3-(23)-jch).

Notes and references

1 H. Peng, L. Zhang, C. Soeller and J. Travas-Sejdic, *Biomaterials*, 2009, **30**, 2132–2148.
2 D. Li, S. P. Song and C. H. Fan, *Acc. Chem. Res.*, 2010, **43**, 631–641.
3 M. Kwak and A. Herrmann, *Angew. Chem., Int. Ed.*, 2010, **49**, 8574–8587.
4 E. Farjami, L. Clima, K. Gothelf and E. Ferapontova, *Anal. Chem.*, 2011, **83**, 1594–1602.
5 S. W. Thomas, G. D. Joly and T. M. Swager, *Chem. Rev.*, 2007, **107**, 1339–1386.
6 H. Peng, L. Zhang, T. H. M. Kjällman, C. Soeller and J. Travas-Sejdic, *J. Am. Chem. Soc.*, 2007, **129**, 3048–3049.
7 X. Z. Zhang, K. Jiao, S. F. Liu and Y. W. Hu, *Anal. Chem.*, 2009, **81**, 6006–6012.
8 G. March, V. Noël, B. Piro, S. Reisberg and M. C. Pham, *J. Am. Chem. Soc.*, 2008, **130**, 15752–15753.
9 Q. D. Zhang, B. Piro, V. Noël, S. Reisberg and M. C. Pham, *Analyst*, 2011, **136**, 1023–1028.
10 X. T. Luo and I. M. Hsing, *Analyst*, 2009, **134**, 1957–1964.
11 S. Pinijsuwan, P. Rijiravanich, M. Somasundrum and W. Surareungchai, *Anal. Chem.*, 2008, **80**, 6779–6784.
12 A. Saghatelian, K. M. Guckian, D. A. Thayer and M. R. Ghadiri, *J. Am. Chem. Soc.*, 2003, **125**, 344–345.
13 L. Wang, Y. W. Zhang, J. Q. Tian, H. L. Li and X. P. Sun, *Nucleic Acids Res.*, 2011, **39**, e37.
14 Y. Wu, S. Liu and L. He, *Anal. Chem.*, 2009, **81**, 7015–7021.
15 H. Korri-Youssoufi, F. Garnier, P. Srivastava, P. Godillot and A. Yassar, *J. Am. Chem. Soc.*, 1997, **119**, 7388–7389.
16 H. Korri-Youssoufi and A. Yassar, *Biomacromolecules*, 2001, **2**, 58–64.
17 C. Riccardi, H. Yamanaka, M. Josowicz, J. Kowalik, B. Mizaikoff and C. Kranz, *Anal. Chem.*, 2006, **78**, 1139–1145.
18 C. Riccardi, C. Kranz, J. Kowalik, H. Yamanaka, B. Mizaikoff and M. Josowicz, *Anal. Chem.*, 2008, **80**, 237–245.
19 H. Q. A. Lê, S. Chebil, B. Makrouf, H. Sauriat-Dorizon, B. Mandrand and H. Korri-Youssoufi, *Talanta*, 2010, **81**, 1250–1257.
20 M. C. Pham, B. Piro, L. D. Tran, T. Ledoan and L. H. Dao, *Anal. Chem.*, 2003, **75**, 6748–6752.
21 S. Reisberg, B. Piro, V. Noe1 and M. C. Pham, *Anal. Chem.*, 2005, **77**, 3351–3356.
22 B. Piro, S. Reisberg, V. Noel and M. C. Pham, *Biosens. Bioelectron.*, 2007, **22**, 3126–3131.
23 S. J. Tian, J. Y. Liu, T. Zhu and W. Knoll, *Chem. Mater.*, 2004, **16**, 4103–4108.
24 J. Wu, Y. H. Zou, X. L. Li, H. B. Liu, G. L. Shen and R. Q. Yu, *Sens. Actuators, B*, 2005, **104**, 43–49.
25 H. X. Chang, Y. Yuan, N. L. Shi and Y. F. Guan, *Anal. Chem.*, 2007, **79**, 5111–5115.
26 K. Arora, N. Prabhakar, S. Chand and B. D. Malhotra, *Anal. Chem.*, 2007, **79**, 6152–6158.
27 L. J. Zhang, H. Peng, P. A. Kilmartin, C. Soeller and J. Travas-Sejdic, *Electroanalysis*, 2007, **19**, 870–875.
28 K. Arora, N. Prabhakar, S. Chand and B. D. Malhotra, *Biosens. Bioelectron.*, 2007, **23**, 613–620.
29 N. Prabhakar, K. Arora, H. Singh and B. D. Malhotra, *J. Phys. Chem. B*, 2008, **112**, 4808–4816.
30 C. Dhand, M. Das, M. Datta and B. D. Malhotra, *Biosens. Bioelectron.*, 2011, **26**, 2811–2821.
31 K. Lee, J. M. Rouillard, T. Pham, E. Gulari and J. Kim, *Angew. Chem., Int. Ed.*, 2007, **46**, 4667–4670.
32 H. A. Ho, K. Doré, M. Boissinot, M. G. Bergeron, R. M. Tanguay, D. Boudreau and M. Leclerc, *J. Am. Chem. Soc.*, 2005, **127**, 12673–12676.
33 W. Zheng and L. He, *J. Am. Chem. Soc.*, 2009, **131**, 3432–3433.
34 S. Liu, L. Wang, Y. L. Luo, J. Q. Tian, H. L. Li and X. P. Sun, *Nanoscale*, 2011, **3**, 967–969.
35 H. L. Li, L. Wang, J. F. Zhai, Y. W. Zhang, J. Q. Tian and X. P. Sun, *Macromol. Rapid Commun.*, 2011, **32**, 899–904.
36 J. Tarver, J. E. Yoo, T. J. Dennes, J. Schwartz and Y. L. Loo, *Chem. Mater.*, 2009, **21**, 280–286.
37 W. Zhang, T. Yang, X. Li, D. B. Wang and K. Jiao, *Biosens. Bioelectron.*, 2009, **25**, 428–434.
38 Y. W. Hu, T. Yang, X. X. Wang and K. Jiao, *Chem.–Eur. J.*, 2010, **16**, 1992–1999.
39 X. X. Wang, T. Yang, X. Li and K. Jiao, *Biosens. Bioelectron.*, 2011, **26**, 2953–2959.
40 J. Wang and A. J. Bard, *Anal. Chem.*, 2001, **73**, 2207–2212.
41 C. Q. Zhang, G. C. Li and H. R. Peng, *Mater. Lett.*, 2009, **63**, 592–594.
42 Y. Ma, K. Jiao, T. Yang and D. X. Sun, *Sens. Actuators, B*, 2008, **131**, 565–571.
43 A. V. Saprigin, C. W. Thomas, C. S. Dulcey, C. H. Patterson Jr and M. S. Spector, *Surf. Interface Anal.*, 2004, **36**, 24–32.
44 S. A. Kumar and S. M. Chen, *Sens. Actuators, B*, 2007, **123**, 964–977.
45 M. Du, T. Yang and K. Jiao, *J. Mater. Chem.*, 2010, **20**, 9253–9260.
46 P. Kavanagh and D. Leech, *Anal. Chem.*, 2006, **78**, 2710–2716.
47 S. A. Kumar and S. M. Chen, *J. Mol. Catal. A: Chem.*, 2007, **278**, 244–250.
48 T. Yang, N. Zhou, Y. C. Zhang, W. Zhang, K. Jiao and G. C. Li, *Biosens. Bioelectron.*, 2009, **24**, 2165–2170.
49 H. Peng, C. Soeller, M. B. Cannell, G. A. Bowmaker, R. P. Cooney and J. Travas-Sejdic, *Biosens. Bioelectron.*, 2006, **21**, 1727–1736.
50 N. K. Chaki and K. Vijayamohanan, *Biosens. Bioelectron.*, 2002, **17**, 1–12.
51 X. Bin and H. B. Kraatz, *Analyst*, 2009, **134**, 1309–1313.
52 S. O. Kelley, E. M. Boon, J. K. Barton, N. M. Jackson and M. G. Hill, *Nucleic Acids Res.*, 1999, **27**, 4830–4837.
53 J. J. Gooding, A. Chou, F. J. Mearns, E. Wong and K. L. Jericho, *Chem. Commun.*, 2003, **3**, 1938–1939.
54 S. O. Kelley and J. K. Barton, *Science*, 1999, **283**, 375–381.
55 J. C. Genereux and J. K. Barton, *Chem. Rev.*, 2010, **110**, 1642–1662.